Biochimica et Biophysica Acta 1814 (2011) 1305–1317

Contents lists available at ScienceDirect

Biochimica et Biophysica Acta

journal homepage: www.elsevier.com/locate/bbapap

Dynamics of polymerization shed light on the mechanisms that lead to multiple amyloid structures of the prion protein ☆

Maria-Teresa Alvarez-Martinez [a], Pascaline Fontes [b], Viviana Zomosa-Signoret [c], Jacques-Damien Arnaud [a], Erwan Hingant [d], Laurent Pujo-Menjouet [d], Jean-Pierre Liautard [c,*]

[a] Institut Fédératif de Biologie de Montpellier (IFR-122), Université Montpellier2, Place E. Bataillon, 34095 Montpellier, France
[b] Centre CECEMA, Université de Montpellier2, Place E. Bataillon, 34095 Montpellier, France
[c] Centre de Recherche sur les Pathogènes et Biologie pour la Santé (CPBS), UMR5236, Université Montpellier2, Place E. Bataillon, 34095 Montpellier, France
[d] Université de Lyon, Université Lyon 1, UMR5208, Institut Camille Jordan 43 bd du 11 Novembre 1918, 69622 Villeurbanne Cedex, France

ARTICLE INFO

Article history:
Received 22 November 2010
Received in revised form 20 May 2011
Accepted 25 May 2011
Available online 16 June 2011

Keywords:
Prion
Amyloid
Heterogeneity
Strain
Dynamics

ABSTRACT

It is generally accepted that spongiform encephalopathies result from the aggregation into amyloid of a ubiquitous protein, the so-called prion protein. As a consequence, the dynamics of amyloid formation should explain the characteristics of the prion diseases: infectivity as well as sporadic and genetic occurrence, long incubation time, species barriers and strain specificities. The success of this amyloid hypothesis is due to the good qualitative agreement of this hypothesis with the observations. However, a number of difficulties appeared when comparing quantitatively the *in vitro* experimental results with the theoretical models, suggesting that some differences should hide important discrepancies. We used well defined quantitative models to analyze the experimental results obtained by *in vitro* polymerization of the recombinant hamster prion protein. Although the dynamics of polymerization resembles a simple nucleus-dependent fibrillogenesis, neither the initial concentration dependence nor off-pathway hypothesis fit with experimental results. Furthermore, seeded polymerization starts after a long time delay suggesting the existence of a specific mechanism that takes place before nucleus formation. On the other hand, polymerization dynamics reveals a highly stochastic mechanism, the origin of which appears to be caused by nucleation heterogeneity. Moreover, the specific structures generated during nucleation are maintained during successive seeding although a clear improvement of the dynamics parameters (polymerization rate and lag time) is observed. We propose that an additional on-pathway reaction takes place before nucleation and it is responsible for the heterogeneity of structures produced during prion protein polymerization *in vitro*. These amyloid structures behave like prion strains. A model is proposed to explain the genesis of heterogeneity among prion amyloid.

1. Introduction

Prions are the unconventional infectious agents responsible for transmissible spongiform encephalopathies, which appear to be composed mainly or exclusively of the misfolded prion protein (PrP^{Sc}). Prion replication involves the conversion of the normal prion protein (PrP^{C}) into the misfolded isoform, catalyzed by tiny quantities of PrP^{Sc} present in the infectious material [1].

The mainstream molecular theory proposed to explain the prion phenomenon is the so-called amyloid formation introduced by Lansbury's team [2,3]. It describes the formation of large aggregates of proteins ordered by specific contacts [4]. The model is based on nucleation-dependent protein polymerization that describes many well-characterized processes, including protein crystallization, microtubule assembly, flagellum assembly, sickle-cell hemoglobin fibril formation, bacteriophage procapsid assembly, and actin polymerization as well as amyloid polymerization. Nucleus formation requires a series of association steps that are thermodynamically unfavorable ($K \ll 1$) because the resultant intermolecular interactions do not outweigh the entropic cost of association [5]. Once the nucleus has been formed, further addition of monomers becomes thermodynamically favorable ($K \gg 1$) because monomers attach to the growing polymer, resulting in rapid polymerization/growth [4]. According to this theory, nucleus formation is the kinetic barrier to sporadic prion diseases that can be bypassed by infection. Nucleus formation is very slow at monomer concentrations slightly exceeding the critical concentration, whereas a small increase in PrP concentration would greatly increase the rate of nucleation [2,3]. It is assumed that

Abbreviations: ATF, Atomic Force; CD, Circular Dichroism; FACS, Fluorescence Activated Cells Sorting; GdnCl, Guanidium Chloride; PrP, Prion protein; rPrP, recombinant prion protein; FTIR, Fourier-transform infrared spectroscopy; ThT, Thioflavin-T

☆ Competing interests: The authors declared no competing interest.

* Corresponding author. Tel: +33 4 67 14 47 46; fax: +33 4 67 14 33 38.
E-mail address: liautard@univ-montp2.fr (J.-P. Liautard).

1570-9639/$ – see front matter © 2011 Elsevier B.V. All rights reserved.
doi:10.1016/j.bbapap.2011.05.016

infection results from seeding of PrP polymerization, by preformed PrP^{Sc} nuclei.

Amyloids are fibrillar protein polymers with a cross-β structure [6]. Polymerization of proteins or peptides into amyloid fibrils occurs during a number of protein deposition diseases but also during the physiological assembly of several microbial proteins into cell surface structures. In the particular case of the prion proteins, amyloids or amyloid-like assemblies become self-perpetuating *in vivo* and thus turn into pathological infectious agents in mammals or protein-based genetic elements in yeast [7].

Amyloid formation appears to be the heart of prion propagation. The isomorphism between prion semiology and amyloid formation should be extended to the molecular mechanisms of strain formation and to molecular mechanisms of species barrier phenomenon. For several years, the existence of prion strains questioned the "protein only" hypothesis of prion diseases. Today, a number of experimental works have clearly demonstrated that structural differences correlate with biological strains [8–11] (see also Refs. [12,13], for recent reviews). Furthermore, besides the natural biological strains discovered during purification of the infectious agent from the brain of infected animals or humans, new strains have been obtained by *in vitro* manipulation of recombinant or purified prion protein [14,15]. However, the question of the molecular mechanisms at the origins of the strains is still unclear. In the present work, we show the appearance of heterogeneous structures during nucleation and their propagation during polymerization. This phenomenon suggests a critical sensitivity to the initial conditions that could explain both the *in vitro* creation of new strains and the stability of biological isolates. We show that this phenomenon takes place during the first step of the reaction, before nucleation.

2. Methods and experimental procedures

2.1. Methods

Protein amyloid polymerization is a complex feature that has received great attention and numerous models have been proposed [4,16–19], a complete review of the models has been recently published [20]. However, most of the models proposed lead to parameters that are difficult to reach experimentally. To avoid this difficulty, we used quantitative models specifically designed to analyze the experimental results we obtained by *in vitro* polymerization of the recombinant hamster prion protein. The simplifications of the original models will be justified by experimental results (see Appendix A and B).

Different quantitative models were used to fit the experimental data. The geometrical meaning of the parameters is depicted in Fig. 1.

2.1.1. As a first general approach

As a first general approach, we used an empirical function to fit a sigmoidal curve obtained by observing polymerization (y) with fluorescent ThT as a function of time (t):

$$y = y_0 + \frac{a}{1 + e^{\frac{t-T_i}{\tau}}} \tag{1}$$

This equation, independent of the amyloid protein type, fits the fibrillation data reasonably well and was shown to have real physical meaning [21]. T_i is the time at the inflection point of the sigmoid and the slope $1/\tau$ of the sigmoid can be identified as a polymerization rate (see Fig. 1). In order to minimize the participation of the polymerization rate in the determination of lag time, we define the lag time (T_{lag}) as proposed by many authors (see Ref. [21]) as a function of Ti and τ.

$$T_{lag} = Ti - 2\tau \tag{2}$$

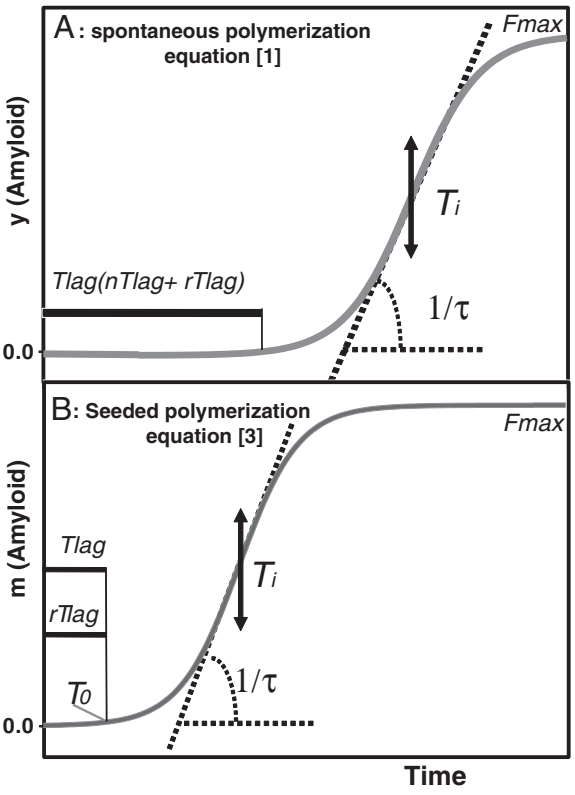

Fig. 1. Schematic representation of the curves parameters obtained from regression analysis. The curves were obtained according to Eq. (1) (panel A) for spontaneous polymerization and to Eq. (3) for seeded polymerization (panel B). The meaning of the parameters is depicted on the figure and the different types of lag times are clarified. *Fmax*: complete polymerization measured as the maximum of fluorescence; *Ti*: inflection point when the rate is maximum, defined in Eq. (1);$1/\tau$: maximum rate of polymerization, defined in Eq. (1); T_{lag}: lag time, defined in Eq. (2); T_0: time at which polymerization starts, defined in Eq. (3); T_{nlag}: genuine lag time resulting from nucleation, defined in Eq. (4) and (A.9); T_{rlag}: residual lag time, experimentally shown to be T_0 in seeding experiments.

We used SigmaPlot 11 nonlinear regression Wizard with the sigmoidal 4 parameters, to obtain a good fit with 5 to 50 iterations. Generally, a correlation coefficient of r>0.99 was obtained.

2.1.2. The exact meaning of lag time

In order to understand what the T_{lag} consist of, we have performed seeded experiments that eliminate the part of the T_{lag} resulting from the formation of nucleus (*i.e.* T_{nlag} as defined in Appendix A). Seeded experiments were analyzed according to the following Eq. (3) derived in Appendix B. It allows the calculation of the time at which polymerization truly begins (T_0) and brings out a residual lag time (T_{rlag}) independent of the nucleation and of the autocatalytic characteristic of polymerization (see Appendix B, for derivation, validation and interpretation of this equation)

$$m = a_0 + \frac{M_0}{1 + \left(\frac{M_0}{m_0} - 1\right)e^{-\frac{k}{N}(t-T_0)}} \tag{3}$$

Where M_0 is the initial concentration of the monomer, m_0, is the concentration of monomers in the polymeric form added for seeding; m is the total number of monomers into amyloid measured by the ThT fluorescence, N is the mean number of monomers in the polymers, T_0, is the time when polymerization truly begins, and $T_{rlag} = T_{lag} - T_0$ is a residual lag time. T_i was measured on the curve. We used SigmaPlot 11 nonlinear regression Wizard with the user-defined Eq. (3), to obtain a

good fit with 5 to 50 iterations. A correlation coefficient of r > 0.99 was always obtained.

2.1.3. We considered then a simplified theory

We considered then a simplified theory, based on the "pre-equilibrium" assumption of Goldstein and Stryer [22], of the nucleation. This theory is introduced in Appendix A (see also Refs. [4,19,23]). A major characteristic of the nucleation theory is the strong dependence of the fibril formation rate on concentration which increases with the size of nucleus (Eq. (A.9)). This concentration dependence can be expressed in terms of T_{nlag} as follows:

$$log\left[T_{nlag}\right] = -(n-1)\,log[M_0] + Constant \quad (4)$$

Where M_0 is the initial concentration of prion protein, and n is the number of subunits in the nucleus.

2.2. Expression and purification of recombinant prion protein

Recombinant 90-231-prion protein (rPrP) from Syrian hamster (*Misocricetus auratus*) provided by SB Prusiner was produced as described previously [24]. Protein concentrations were determined spectrophotometrically (Beckman spectrophometer) using an extinction coefficient of 25 327 M^{-1} cm^{-1} at 278 nm and a molecular mass of 16,227 kDa. Purity of the protein preparation was assessed by phase reverse HPLC. The protein was stored lyophilised at −80 °C.

2.3. Preparative in vitro polymerization

Samples containing 0.4 to 1.2 mg/ml of the oxidized form of HaPrP90-231 (rPrP) were incubated for 1–5 days with 50 mM sodium acetate, pH 4.0, 0.5 M GdnHCl (Buffer A) or pH 6.8 in phosphate-buffered saline (PBS), 1 M GdnHCl, 2.44 M urea, 150 mM NaCl (Buffer B), or 50 mM MES, pH = 6.0, 2MGdnHCl (Buffer C) [25]. The rPrP spontaneously converted into the fibrillar isoform upon continuous shaking at 250 rpm in conical plastic tubes (Eppendorf) in a reaction volume 1.3 ml at 37 °C (lying down Tube). In some cases, polymerization was obtained upon continuous shaking at 600 rpm using a Thermomixer comfort (Eppendorf) in conical plastic tubes (Eppendorf) in a reaction volume 0.4 ml at 37 °C (upright Tube). To monitor the kinetics of fibril formation aliquots were withdrawn and diluted 100-fold into PBS to a final concentration of rPrP of 4 μg/ml. After the addition of thioflavin T (ThT) (Sigma) to a final concentration 10 μM for 5 min. the fluorescence measurements were performed at room temperature with a FluoroMax-2 fluorimeter (Jobin Yvon-Spex, Tokyo, Japan) with a 10.4 mm path length rectangular cuvette. ThT emission spectra were recorded after excitation at 450 nm (excitation and emission slit widths, 4 nm), each emission spectrum (slit width, 4 nm) was the average of three scans.

2.4. Transmission electron microscopy

Samples were absorbed on carbon/formvar-coated copper grids (300 mesh) (Agar scientific, Saclay, France) and stained by negative contrast with 2% (w/v) uranyl acetate for 1 min. Labeled samples are observed after negative contrast with uranyl acetate 2% on a JEOL 1200 EX II transmission electron microscope (Service commun de microscopie électronique de l'université Montpellier II, Montpellier, France) at 80 kV of voltage. Length and width of fibrils were measured with ImageJ software (http://rsbweb.nih.gov/ij/).

2.5. Fluorescence microscopy

Samples were diluted in sodium acetate 50 mM buffer pH5 containing 10 μM Thioflavin T (ThT). Images acquisition was performed on an inverted Leica DM IRB microscope equipped with a Leica DFC350 FX digital camera at gross x945. Images were analyzed with Adobe Photoshop and ImageJ software.

2.6. FACS analysis

Flow cytometric analysis of aggregates was performed as described [26]. Measurements were made using a FACScalibur (Becton Dickinson) with Cell Quest software. 1 ml of a fibril suspension at 2.4 μM final and placed in the flow cytometer; 10,000 data points were acquired for subsequent analysis. The thioflavin-T, assays were performed by adding a freshly prepared stock solution to the protein samples to final thioflavin-T concentration of 10 μM. Samples were allowed to reach equilibrium for 5 min before data collection. The fluorescence intensity of ThT (FL1), collected during the second acquisition, was then plotted *versus* particle size measured by side scattering (SSC).

2.7. FTIR and CD analysis

CD spectra were recorded at ambient conditions using a J810 spectropolarimeter (Jasco). A 0.1-cm optical path length quartz cell was used to record spectra of proteins in the far UV region (190–260 nm). Protein concentration and buffers were those used in the UV absorbance experiments. Baseline corrected CD spectra were acquired at a scan speed of 20 nm min^{-1}, a 1-nm bandwidth, and a response time of 1 s. The sample compartment was purged with pure dry nitrogen. Spectra were signal-averaged over four scans.

The IR spectra were obtained with a Bruker (Ettlingen, Germany) Vertex 80v FTIR spectrometer equipped with a liquid-nitrogen-cooled, broad-band, mercury–cadmium telluride solid-state detector. The spectra (100 scan accumulation) were co-added after registration at a spectral resolution of 2 cm^{-1} and analyzed with the Opus 6.0 program. For comparison of soluble and aggregated protein, all spectra were recorded with dry samples. After the isolation of aggregates by centrifugation (22 psi ≈ 127,000 g for 60 min, airfuge air-driven Micro-ultracentrifuge Beckman Coulter), and suspension in corresponding buffer, the sample was deposited onto a CaF2 plate, and the solvent was allowed to evaporate overnight at room temperature. To compare qualitatively the spectra of different samples, each spectrum was normalized with respect to the integrated intensity of the entire spectrum.

2.8. Kinetic measurements of polymerization

The kinetics of amyloid formation was monitored in SpectraMax Gemini XS (Molecular Devices). Samples containing 0.1 to 1.2 mg/ml of the oxidized form of HaPrP90-231 (rPrP) were incubated in Buffer A, Buffer B or Buffer C upon continuous shaking at 1350 rpm in 96-well plate and in the presence of ThT (10 μM). The kinetics was monitored by bottom-reading of fluorescence intensity using 445 nm excitation and 485 and 500 nm emission. Every set of measurements was performed in triplicates, and the results were averaged. Seeding was performed by adding a percentage of previously prepared amyloid and the w/w percent was calculated assuming that suspension was homogeneous.

3. Results

3.1. Prion-amyloid formation under different incubation conditions follows similar dynamics

The goal of the present work was to shed light on the mechanisms involved in the dynamic and the generation of heterogeneity during the formation of different structural types of amyloids of the prion protein. Amyloids formation is obtained from partially unfolded proteins [27]. As a first approach, we took advantage of this observation to use three buffers that induce different denaturation stages of the native prion protein. Analysis was performed by Circular Dichroism (CD). The secondary structure of the prion protein in buffer B is mainly under the

alpha-helix conformation. The comparison of the CD spectrum obtained in buffer B with the one observed in benign buffer (*i.e.* PBS) shows that the prion protein conformation remains mainly under alpha helix when transferred into this buffer B. On the other hand, the CD spectrum obtained in buffer A evidenced a major change in the secondary structure with a loss of α-helix and a dramatic increase of the random coiled proportion in the molecule (see Ref. [24]).

To obtain amyloid formation we incubated the recombinant prion protein at different concentrations (0.1 mg/ml to 1.2 mg/ml) and different temperatures (between 20 °C and 37 °C), and in each buffer (*i.e.* in buffers A, B and C). Amyloid formation was monitored by thioflavin-T (ThT) fluorescence. The resultant curves were analyzed as described in Methods. The parameters deduced are presented in Fig. 1.

Fig. 2A and B shows some independent kinetics of the amyloid formation under two buffer conditions (*i.e.* Buffers A and B) at a concentration of 0.4 mg/ml. As expected, the kinetics of polymerization obtained under the two buffer conditions gave qualitative similar results, *i.e.* the experimental results can be well approximated by the sigmoidal curve of the Eq. (1) with correlation coefficient R>0.99. (See Fig. 1 for a definition of the geometrical representation of the parameters that were extracted from the experimental curves).

3.2. Polymerization dynamics reveal a highly stochastic mechanism originating from the heterogeneity of nucleation

The first observation that can be worked out from the kinetics curves obtained (Fig. 2) is the heterogeneity of the maximum of fluorescence. Maximum fluorescence varied in the range of five folds. It should be stressed that these values fluctuated in a single experiment between wells of the same plate and there is no correlation with the position on the plate. These observations can be interpreted in three ways: 1/either only a part of the monomers are polymerized or 2/the existence of an irreversible off-pathway that extract the protein to an amorphous aggregate or 3/the fluorescence of ThT differed from one preparation to another. The first hypothesis was tested by measuring the quantity of monomers remaining in the supernatant after centrifugation of the aggregates. Although fine differences have been seen, no systematic differences can be correlated with the fluorescence (results not shown). A consequence of the second proposition would be the existence of a relation between the maximum of fluorescence (*Fmax*) and the T_{lag} and/or τ, the irreversible off-pathway leading to an apparent decrease of the initial concentration thus increasing lag time. No such relations were observed (Fig. 2C and D). On the other hand, a FACS analysis clearly showed that polymers can be differentiated by their ThT binding capacity as shown by the ratio between fluorescence and size of the amyloids (Fig. 3). We thus concluded that different polymers exhibiting different ThT binding properties could be spontaneously formed during polymerization *in vitro*.

To confirm the reality of heterogeneity, we first analyzed the dynamics of the polymerization. The characteristic sigmoid curve can be interpreted according to Eq. (1) to compute a lag time (T_{lag}) and a rate of polymerization ($1/\tau$) (see Methods and experimental procedures). A major observation of a systematic study of the T_{lag} is its heterogeneity both when different buffers are compared but also within a same buffer

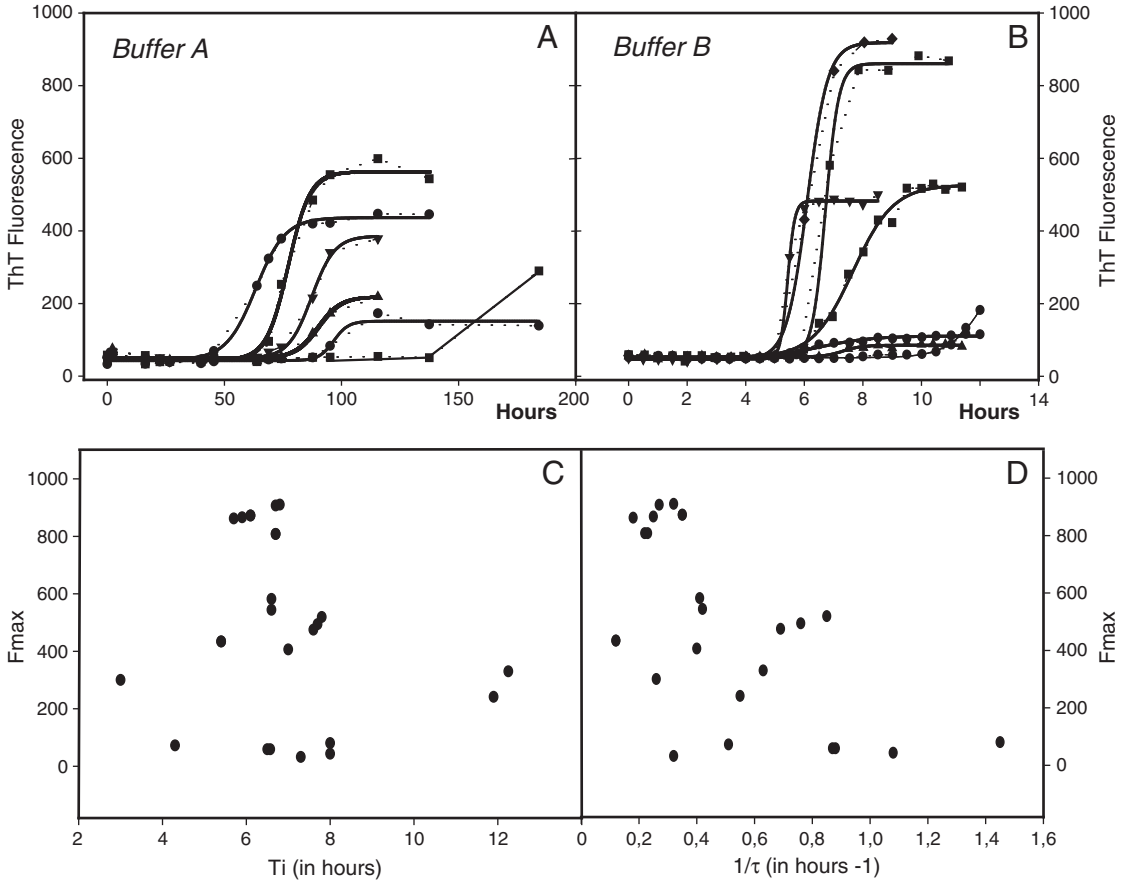

Fig. 2. Heterogeneity of the kinetics of polymerization of rPrP. Samples containing 0.4 mg/ml of the oxidized form of HaPrP90-231 (rPrP) were incubated in Buffer A (panel A) or Buffer B (panel B) upon continuous shaking as described in Experimental procedures. The symbols were chosen different for clarity; the samples were taken from different wells but all in the same plate. The experimental points were used to perform a non linear regression using Eq. (1). The results are representative of a great number (several dozen) of experiments. The maximum fluorescence was plotted against T_i (panel C) and $1/\tau$ (panel D) obtained from regression according Eq. (1). Polymerization depicted in panels C and D was performed in buffer B.

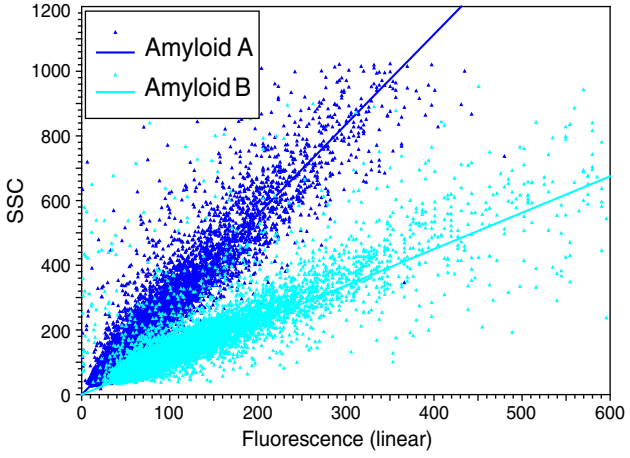

Fig. 3. FACS analysis of the fibrils labeled with ThT. Two different preparations, of amyloids obtained in buffer A and buffer B, were analyzed by FACS as described in Experimental procedures. Each point is put on the figure as a function of size (SSC) and ThT fluorescence.

condition (see Fig. 2). However, the lag time depends on the initial concentration of monomers and the apparent dispersion of the measurement decreases when concentration increases (Fig. 4A). These two results seem qualitatively in agreement with a nucleation dependent mechanism of polymerization. In order to rationalize this observation, we decided to compute the number of monomers in the putative nucleus using the relation (Eq. (4)) described in Methods and mathematically developed in Appendix A. Surprisingly the number of monomers determined according to this theory is only between 1.8 and 2.2, a result hardly consistent with the nucleation theory, particularly to explain the many years long incubation times observed in the sporadic forms of the CJD disease. Such an astonishing result has been previously observed by Baskakov and Bacharova [25] for mammalian prion protein, by Collins et al. [28] for yeast prion, by Chen et al. [29] for polyglutamine or Padrick and Miranker [30] for Islet Amyloid (IAPP). These observations were interpreted either as the existence of an off-pathway for the prion polymerization [25,28] or as a more complex kinetics for IAPP [30]. Although, odd structures have been observed with high resolution microscopy of prion amyloids [25], the existence of an off-pathway can only be ascertained by an analysis of the kinetic data. Three tests have been proposed to ascertain the existence of an off-pathway [31], 1/the dependency of the T_{lag} on initial concentration (Fig. 4); 2/a fit obtained with light scattering (not feasible here) and 3/the improvement of the fitting of the first part of the kinetic while initial concentration increases. Thus we performed a study of the fitting of the first half part of the polymerization curve to the equation proposed by Powers et al. [31]:

$$Y = at + bt^2 + c$$

where *a, b, c* are constants, *Y* is the fluorescence measured at time *t*. We found that the correlation coefficient did not improve when higher concentration of monomers was used (see Supplementary data Fig. S1). This result, together with independence of T_{lag} to maximum fluorescence (Fmax) (Fig. 2C and D), seems to rule out the existence of an off-pathway under the conditions used during these experiments. However, due to the low sensitivity of this test, we decided to address this question by another way. Indeed, another approach to explain the relation between T_{lag} and the monomer concentration is to understand what the lag time consists of in our experiments. We thus decided a thorough analysis of the lag time.

3.3. What is the meaning of apparent T_{lag} in seeding experiments?

In order to investigate the nature of lag time, let us denote T_{lag} as the time before the beginning of observable polymerization according to Eq. (2). In seeding experiments, the T_{lag} does not depend on nucleation (this is clear precisely because of seeding) and thus, T_{lag} should reflect only the sigmoid kinetics that results from an autocatalytic reaction (see Discussion and theory proposed Appendix B). As a consequence, increasing the quantity of seed should result in the complete disappearance of this lag time (T_{lag}). (See for instance Refs. [16,21,32]). This absence of lag time after seeding was observed with numerous proteins that undergo an amyloid polymerization, for instance insulin [33], the beta-peptide of Alzheimer disease [34,35] or the polyglutamine of Huntington disease [36].

In order to test this inference, we have performed an experiment by increasing the seed concentration. The results presented in Fig. 5A invalidate this hypothesis for *in vitro* prion polymerization. Indeed, even at very high concentration of seeds (*i.e.* >10%) an apparent lag time is still obtained suggesting that another phenomenon is responsible for at least a part of this occurrence. As expected (see Eq. (B.9) of Appendix), the decrease of T_i is correctly approximated by

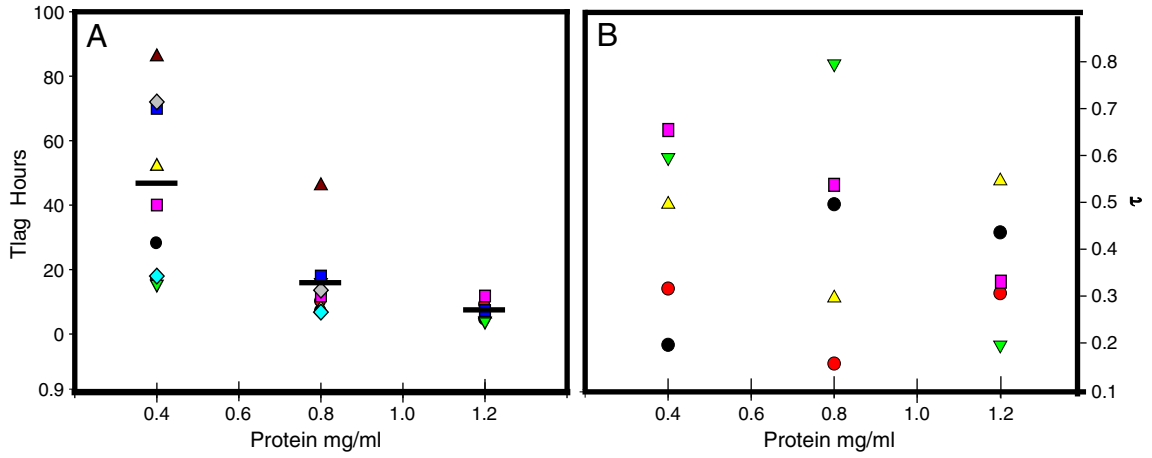

Fig. 4. Lag time (T_{lag}) and rate (τ) dependency of the initial concentration of monomeric rPrP. Kinetics analyses were performed as described in Experimental procedures. Kinetics of amyloid polymerization of rPrP at different concentrations in buffer A at room temperature was obtained in a single experiment (a 96-well plate). Experimental points were used to perform non linear regression using Eq. (1), all the correlation coefficients were greater than 0.99. T_{lag} was calculated according to Eq. (2) (panel A) and τ was deduced directly from Eq. (1) (panel B).

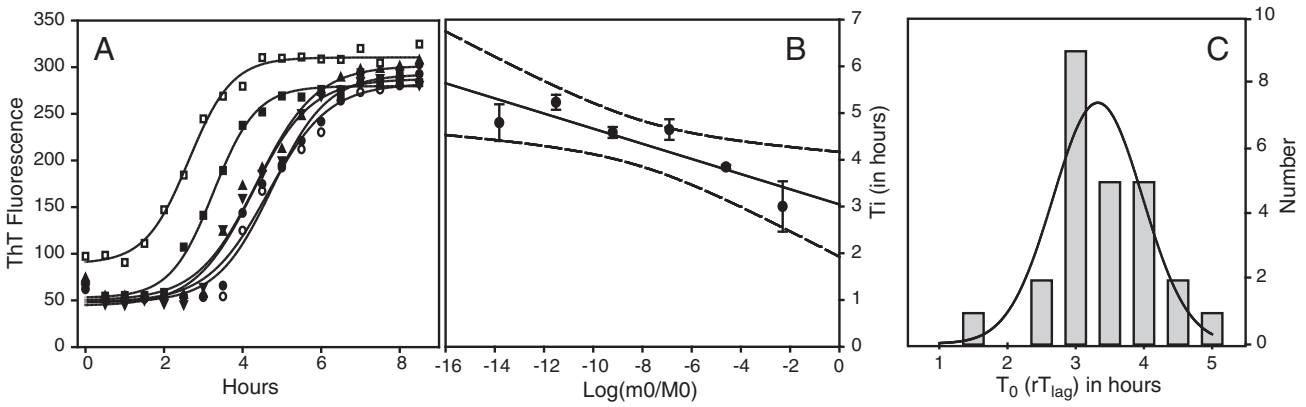

Fig. 5. Lag time did not disappear when seed concentration increased. Kinetics analyses were performed as described in Experimental procedures. Kinetics of amyloid polymerization of rPrP at 0.4 mg/ml in buffer B at room temperature was obtained in a 96-well plate after seeding with m_0 mg/ml of amyloid prepared as described in Experimental procedures. Experimental dots were used to perform nonlinear regression using Eq. (1), all the correlation coefficients were greater than 0.99. T_i was obtained according to Eq. (1). Panel A represents one set of curves obtained among 3 in each experiment. Panel B represents the dependency of T_i against seed quantities in case of polymerization induced by seeding. M_0 is the initial concentration of the monomer and m_0, is the concentration of monomers in the polymers added to seed the reaction. As a consequence, when $m_0 = M_0$, $Log\ (m_0/M_0) = 0$, thus the value of T_i obtained at this point represents the delay necessary to begin polymerization. Panel C shows the delay of polymerization measured by T_0 (Eq. (3)). Kinetics experiments were performed as described in Experimental procedures. Kinetics of amyloid polymerization of rPrP at 0.4 mg/ml in buffer B at room temperature was obtained in a 96-well plate after seeding 0.004 mg/ml of amyloid prepared in the same buffer as described in Experimental procedures. Experimental points were used to perform non linear regression using Eq. (3), all the correlation coefficients were greater than 0.99. T_0 was obtained as a parameter of the regression. The curve represents a normal distribution obtained by regression of the T_0 of the experimental values ($r = 0.89$).

a function of the logarithm of the seeding ratio, and the curve intersects the T_i axis around 3 h (with a 95% probability to be between 2 and 4 h) (Fig. 5B). This value could correspond to a residual lag time (T_{rlag}, see Fig. 1B) under the experimental conditions involved. In order to study the mechanisms responsible for this delay, we have developed a model of polymerization that allows us to identify the parameters of the equations obtained (see Methods and Appendix B). In Eq. (3), the contribution of seeding inside the delay time before polymerization is targeted. Indeed, as detailed in Appendix B, T_0 is the time when seeded polymerization truly begins. Thus, when different from zero, T_0 is a residual lag time (T_{rlag}) not explained by polymerization kinetics. An analysis of the distribution of T_0 confirms that a residual lag time with a mean of 3.3 +/− 0.15 h was necessary before polymerization starts (Fig. 5C). This value (3.3 +/− 0.15 h) is in good agreement with the one (3 +/− 1 h) found by an independent method described above and presented in Fig. 5B. This implies that a time dependent sufficiently long process (*i.e.* 3 h under our experimental conditions) precedes the beginning of polymerization induced by seeding.

Many hypotheses can explain such a phenomenon; however, a simple one would be the existence of a conformational change (see Supplementary data Fig. S2 for a numerical simulation of this hypothesis). Consequently, we decided to test the possibility that a time dependent conformational change leading to an amyloid competent isoform is necessary to begin polymerization. We thus performed an experiment of a delayed seeding to test the possibility that this conformational change comes from the monomer. The results (here with buffer B) show that delayed seeding decreased the lag time but, as a surprise, did not result in its complete disappearance (Fig. 6A and B). The time dependency of the T_{rlag} was well approximated by an exponential curve ($r > 0.98$) that leaves another residual lag time (T_{rrlag}) of 1.7 +/− 0.3 h when seeding is performed at 1% and 1.10 +/− 0.4 h when seeding is performed at 10%, suggesting that a complex mechanism was involved. Two hypotheses can be made to explain such a result: 1/either amyloid seeds undergo conformational change; 2/or monomer conformational change results from a complex mechanism involving many different steps during conformational changes and one of these steps needs interaction with amyloid.

We tested the first hypothesis: did the amyloid change its structure during the seeding process? In order to investigate this possibility, we decided to fix, with formaldehyde the amyloid before seeding. Fixation (*i.e.* chemical cross-linking) of the amyloid did not change the dynamics parameters of polymerization (see Supplementary data Fig. S3). Thus, major structural changes of the seeds were not necessary to start polymerization, leaving as sole explanation a complex mechanism of polymerization that involved monomers. However, any mechanisms involving the monomer should be sensitive to concentration. To challenge this possibility, we decided to change the concentration of monomers ($rPrP^C$) but kept the same quantity of seeds. A numerical simulation of this experiment, with the simple conformational change hypothesis (a change of conformation is necessary to incorporate monomers into polymers) shows that T_i and consequently T_{lag} should decrease when monomer concentration increase (see Supplementary data Fig. S4). On the contrary, the experimental results shown in Fig. 6C clearly exhibit an increase of the apparent lag time with respect to the monomer concentration. Thus, a new hypothesis is needed to be added. We then propose that many conformations could co-exist. Some of them would interact with the amyloid polymers but could not polymerize (see model Fig. 11). In order to validate this model, we investigated the consequences of this proposition.

3.4. Heterogeneity of the nucleation process explains dynamics of polymerization

As a consequence of the model proposed above, the nucleation can start with different protein conformations. This hypothesis is sustained by the observation of the dispersion of the T_{lag} (see for example Figs. 2 and 4) that suggests that the reaction is randomly sensitive to the initial conditions *i.e.* the first nucleus formed will dictate the dynamics and probably the polymers structure. As a consequence, various nuclei could be formed independently resulting in heterogeneity of different polymers (see Figs. 2 and 3). This is also obvious when comparing parameters of the kinetics (*i.e.* T_{lag} and $1/\tau$) (see Fig. 4). Fig. 4B shows that the apparent polymerization rate (τ) is widely dispersed not only between buffer conditions but also within the same buffer. Furthermore, the apparent rate of polymerization is totally independent of the initial concentration (Fig. 4B). This result can also be interpreted as heterogeneity of nucleation and subsequent polymer formation. It can be suggested that different nuclei generated structurally different polymers each exhibiting specific polymerization dynamics.

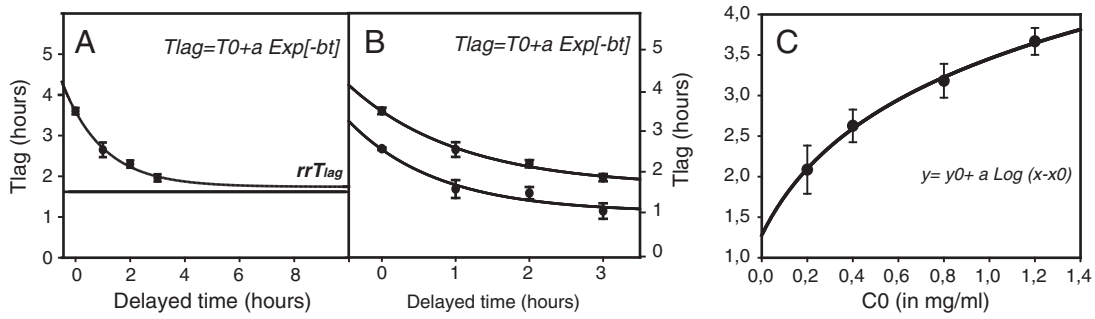

Fig. 6. A and B. Delayed seeding reduced apparent lag Time (T_{lag}) but did not conceal it. Kinetics analyses were performed as described in Experimental procedures. Kinetics of amyloid polymerization of rPrP at 0.4 mg/ml in buffer B at room temperature was obtained in a 96-well plate. Samples were incubated 0, 1, 2 or 3 h before seeding with either 0,004 mg/ml (panels A and B) or 0.04 mg/ml (panel B) of amyloid prepared in the same buffer as described in Experimental procedures. Amyloid polymerization was measured by ThT fluorescence. Experimental points were used to perform non linear regression using Eq. (1) of Experimental procedures, all the correlation coefficients were greater than 0.99. T_{lag} was calculated according to Eq. (2) of Experimental procedures. The points are the average of three independent measurements. We used an exponential function (see figure) to join the points ($r>0.98$). C. Increasing initial concentration of monomers while the concentration of seeding polymers was kept constant resulted in an increase of T_{lag}. Kinetics analyses were performed as described in Experimental procedures. Kinetics of amyloid polymerization of rPrP in buffer B at different concentration was obtained in a 96-well plate after seeding 0.004 mg/ml of amyloid prepared in the same buffer as described in Experimental procedures. Experimental points were used to perform non linear regression using Eq. (1) in and T_{lag} calculated according to Eq. (2), all the correlation coefficients were greater than 0.99. The points are the mean of 4 independent measurements. We used an exponential function to join the points ($r>0.99$).

3.5. Electron microscopy analysis confirms heterogeneity of polymer structures

A straight-forward consequence of the previous experiment suggested that structural differences in nucleus formed should lead to polymer heterogeneity. This latter effect should then be observed by microscopy. The polymers, labeled with ThT, have been first observed by fluorescence microscopy. (Samples of the images are shown as Supplementary data Fig. S5). Indeed very different aspects can be observed, from genuine individual fibrils to huge aggregates where no fibril can be individually distinguished. However, the resolution of optical microscopy, although allowing a large number of sample analyses, cannot distinguish fine structures of the polymers. We thus completed this study by electron microscopy analysis. Many individual experiments reveal specific type of structures even if in some cases the structures look alike (Fig. 7). Heterogeneity of the polymers, between the preparation and eventually between buffers is the main observation. A quantitative analysis of the polymers width clearly confirmed the dispersion of the parameters characterizing the structure of the polymers (Supplementary data Fig. S6).

3.6. Successive seeding allows the selection of more "efficient" amyloid strains

The existence of a structural heterogeneity and the corresponding dynamics parameters have numerous consequences that can be used to better characterize the mechanisms involved. For instance, the results presented above suggest that, in some cases, the apparent rate of polymerization is a mix of many independent rates resulting from the combination of structural and dynamical different amyloids (see Fig. 7 and Supplementary data Fig. S6). A question arises from this observation: What are the effects of repetitive seeding on this heterogeneous mix? After seeding a solution of monomers, two main parameters (See Appendix) direct the polymerization dynamics: 1/the

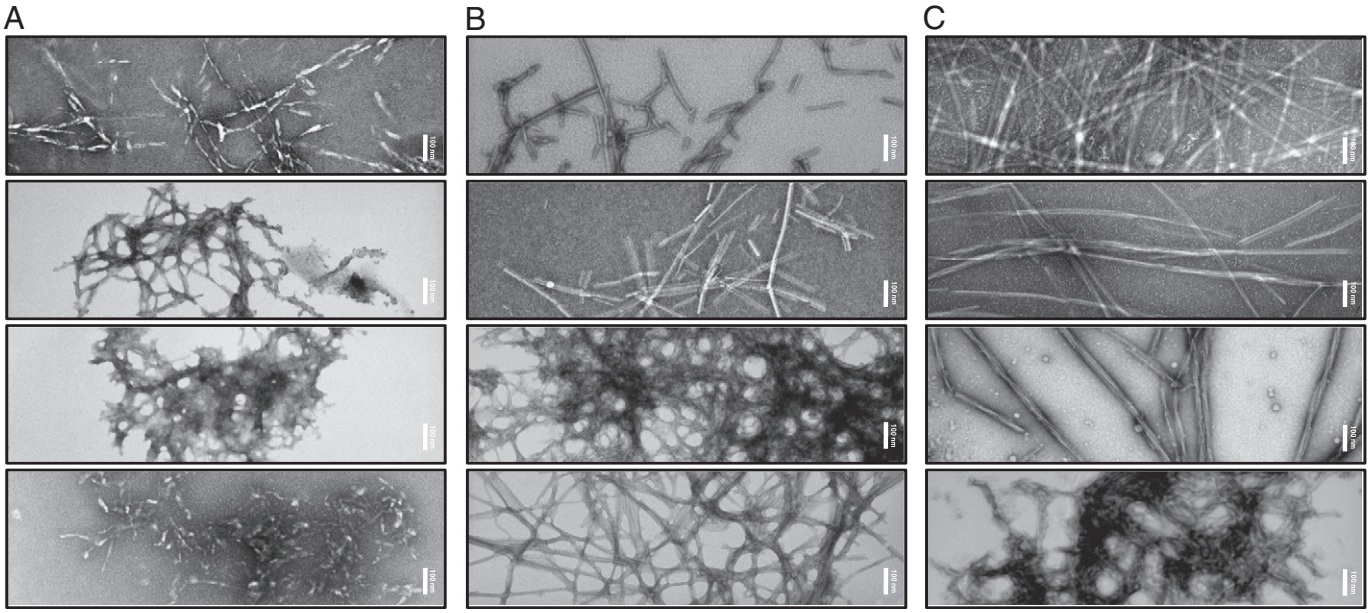

Fig. 7. Electron microscopy analysis confirms the heterogeneity of the amyloid structures. Aliquots of sample obtained after polymerization in buffer A (panel A) or buffer B (panel B), or buffer C (panel C) were proceeded as described in Experimental procedures for examination in negative stain by Electron microscopy. The images represent an arbitrary selection among many different structures that were observed during this work. Scale bars represent 100 nm.

number of nuclei and 2/the polymerization rate (1/τ) (sensitivity of the polymer to splitting is included in this parameter by the mean length N in Eq. (3)). However, it is quite clear that repetitive seeding will favor the fastest polymerization structures (including true polymerization rate (k), and sensitivity to splitting (N), *i.e.* k/N in Eq. (3)) leading to a selection of the amyloid fittest to the buffer conditions and agitation used. We thus decided to produce prion-amyloid by repeating seeding and to analyze the kinetic characteristics of the polymerization.

We thus designed an experiment to test the effect of successive seeding on the kinetics of amyloid formation in buffer B. The results evidenced that successive seeding increased the polymerization rate and decreased the T_{lag} strengthening the hypothesis that a selection operates on a heterogeneous population (Fig. 8). According to Pedersen et al. [37], survival-of-the-fittest would be the mechanism causing the preferred amyloid molecular packing that correlates with the conditions present under fibril formation. However, an increase of polymerization rate could also reflect a mechanism of better packing, for instance by zipping a longer beta-core structure, a kind of adaptation.

3.7. Successive seeding in the same buffer conserved the strain characteristics

Another consequence of the heterogeneity of the structure obtained would be the conservation of the nucleus structure during successive seeding. It should be pointed out that such a result would be in conflict with the thermodynamical hypothesis. Indeed, it was suggested by Pedersen et al. [38] using glucagon as model that, under specific conditions, the structure reached by the amyloid is always the same, the one of the minimal energy (a kind of generalization of the Anfinsen principle). This implied that the formation is thermodynamically driven. To decide between these two hypotheses, we selected two preparations that exhibit noticeably different parameters (*i.e.* ThT binding and dynamics characteristics) and we used these two samples to seed successively independent preparations. The results obtained with buffer B are presented in Fig. 9, the kinetics characteristic (*i.e.* T_{lag}, τ and fluorescence) and the ThT binding properties remain approximately the same during three successive seedings. To confirm this observation, we have compared the amyloid structure by electron microscopy (see Supplementary data Fig. S7). These results suggest that, at least for a few successive seeding, nucleation is predominant on determining the kind of structure that is selected and thus seeding conserved the specificities of the amyloid, something reminiscent of the strains phenomenon. However, due to the few number of successive seedings, these observations cannot rule out the thermodynamic fate of the system according "the Ostwald step rules" (see Ref. [39]).

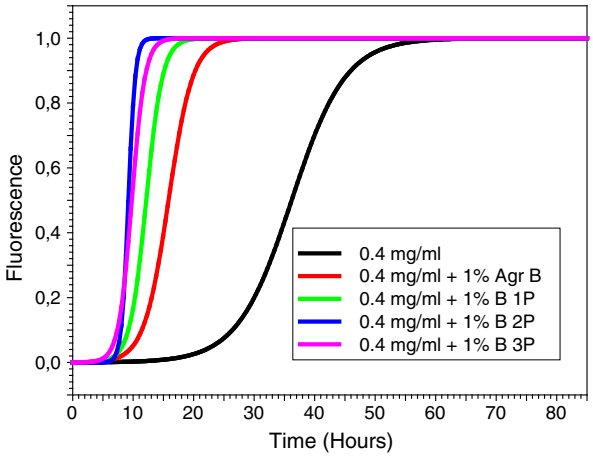

Fig. 8. Repeated seeding leads to a decrease of T_{lag} and an increase of the apparent rate of polymerization (1/t). Kinetics of amyloid polymerization of the rPrP at 0.4 mg/ml in buffer B at room temperature was obtained in a 96-well plate. The experimental results were used to perform non linear regression according to Eq. (1) of Experimental procedures. They were normalized in order to clearly evidence that the Tlag and speed polymerization. The first kinetic (black line) was obtained without seeding. All the other curves were obtained after seeding at 0.004 mg/ml using the previous amyloid as presented on the figure.

3.8. For prion, fibril nucleation and elongation do not involve similar molecular mechanisms

A consequence of the predominance of the nucleus directed polymerization could be a discrepancy between kinetic parameters polymerization and nucleus formation dynamics. Previous studies of amyloid formation *in vitro* using insulin, glucagon, β2-microglobuline and different variants of Aβ (1–40) as model systems have shown that the length of the lag time and the elongation rate are correlated [32,40,41]. To determine whether this is the case for the rPrP used here, the elongation rate (1/τ) and the lag time (T_{lag}) for individual samples of some variants studied were plotted (Fig. 10). As expected from the model deduced from the previous experiments, the results revealed a complete absence of correlation between these two parameters, suggesting a predominance of nucleation parameters in the determination of T_{lag}. This observation indicates a different mechanism of trans conformation of the monomer during fibril nucleation and elongation. This result seems completely different from those obtained with other peptides and proteins [32,40,41], suggesting that prion fibrillation takes a specific way not common to other amyloid formation. However, this is not a fundamental discrepancy but only a different experimental point of view (see Discussion).

4. Discussion

Although prion protein aggregation has been studied for quite a long time, a number of fallacies persist. Probably the most notable is the assumption that a lag time in the kinetics represents a nucleation phase and that the end of such a lag corresponds to cessation of nucleation. This idea was challenged by experimental results obtained by numerous authors that reveal a linear dependency of the T_{lag} with monomer concentration not exceeding a nucleus size of n~2. This result, also found for some other amyloid-forming proteins, is challenging for the nucleation theory of prion that was introduced to explain very long delay time before onset of the disease. *In vitro*, this low number of monomers found in the nucleus was generally attributed to an accumulation of large off-pathway species whose formation is competitive with the on-pathway processes that leads to amyloid [25,42,43]. However, in many cases off-pathway appears as an *ad hoc hypothesis* that was difficult to sustain by experimental results, the evidence of odd structures on electron microscopic image cannot be unambiguously interpreted as off-pathway. In some cases, a more complex pattern of the polymerization process was used to explain the complex dynamics of amyloid formation, as for instance the 'Nucleated Conformational Conversion' (NCC) of yeast prion element [PSI+] [44] or the dispersed phase-mediated fibrillogenesis (PMF) for amylin [30]. In the case of hamster rPrP polymerized *in vitro*, we found no kinetic evidence for an off-pathway, thus, we proposed that an additional path, on-pathway, is necessary to explain the results observed (see Fig. 11 for a schematic representation). This is probably a first step, before nucleation, because we showed that seeded polymerization begins after a delay-time (3 h when considering our experimental conditions) that can be interpreted as the generation of active monomers, resulting probably from a change in spatial structure. Thus, the results presented here can be explained by a complex mechanism that directs conformational changes leading to structural competent monomers. Because the conformational change takes about 3 h under the experimental conditions we used here; it cannot be a simple protein 'breathing' that needs only a small fraction

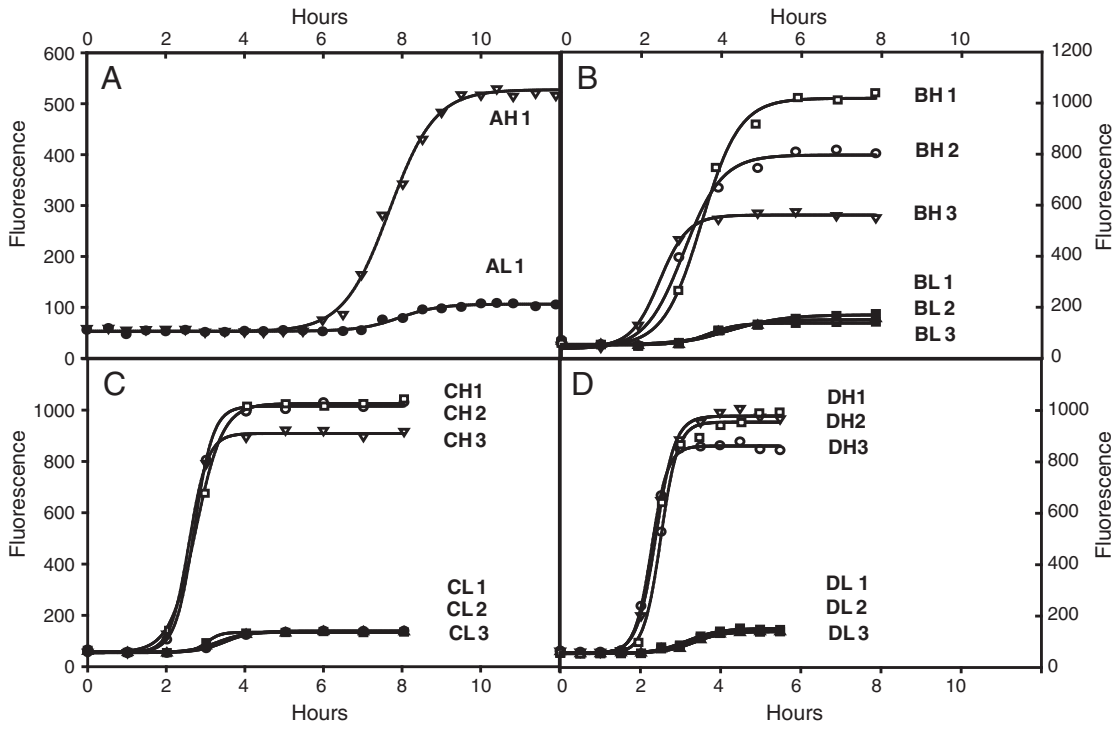

Fig. 9. While decreasing T_{lag} and increasing apparent rate of polymerization ($1/\tau$), strain-maintained during repeated seeding. Successive seeding experiments were performed as follows: amyloid polymerizations of rPrP were obtained at 0.4 mg/ml in buffer B at room temperature in a 96-well plate. A set of polymerization was first performed without seeding and two preparations with very different characteristics (*i.e.* Maximum fluorescence, rate of polymerization and lag time) were selected (panel A). They were called AH1 (Figure A, High fluorescence, sample 1) and AL1 (Figure A, low fluorescence, sample 1). Three aliquots of each were used to seed polymerizations with the same concentration of rPrP (0.4 mg/ml) in the same buffer B. Three independent seeding were done. The kinetics is presented in panel B. BH1, BH2 and BH3 were obtained by seeding with AH1 and BL1, BL2 and BL3 were obtained by seeding with AL1. Experiments were carried on by seeding polymerization with preparation BH1 and BL1. The kinetics obtained is presented in panel C. Finally preparation CH1 and CL1 were used to seed a last polymerization, the kinetics of which are presented in panel D. The experimental results were used to perform non linear regression according Eq. (1) of Experimental procedures.

of a second as for instance in polyglutamine [36]. In the model depicted in Fig. 11, this step is symbolized by a black-box. Unconventional initiation steps of the reaction preceding polymerization have been proposed to explain complex behavior in amyloidogenesis. In the case of polyglutamine this was interpreted as a simple conformational change [36], but, in this model, seeding results in a complete disappearance of the T_{lag}. For α-synuclein the dynamics

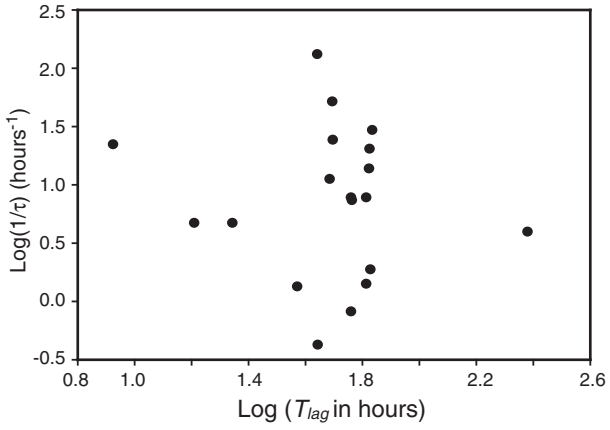

Fig. 10. Under the experimental conditions used, no correlation between apparent rate of polymerization ($1/\tau$) and T_{lag} can be observed. Kinetics of amyloid polymerization of rPrP at 0.4 mg/ml in buffer A at room temperature was obtained in a 96-well plate. Fluorescence was regularly monitored as described in Experimental procedures. Experimental points obtained were used to perform nonlinear regression using Eq. (1), all the correlation coefficients were greater than 0.99. τ was deduced directly from Eq. (1) and T_{lag} was calculated according to Eq. (2).

was interpreted as a fibrillation process in which oligomeric granular species turn into amyloid fibrils through concerted lateral association of the preformed granules [45], amylin polymerization was also shown by ATF microscopy to result from the association of oligomers [46]. Evidence of the existence of micelles during the fibrillogenesis of beta-amyloid peptide has also been published [47,48]. Taken into account the results we present, we suggest that the time before polymerization is linked to the production of multiple conformations. The molecular mechanisms that sustain this process in the case of hamster rPrP are under investigation.

Structural heterogeneity of the amyloid polymerized from a highly purified protein is a well-established fact [49–52]. A cross-β sheet structure set up the core of amyloid protofilaments that represents the filamentous substructures of mature fibrils. Although the basic structural arrangement of the cross-β structure is conserved for different fibrils, there are different possibilities for them to pack into the three-dimensional fibril structure. Such variable protofilament arrangements can give rise to several distinct amyloid fibril morphologies that were recently unraveled at the atomic level [53]. Structurally polymorphic amyloid fibrils are not only reported for *in vitro* preparations. Examination of several tissue-extracted amyloid fibrils shows also significant structural polymorphism [54]. In prion diseases, the strain phenomenon has been correlated with difference in structure of the associated amyloid [8–11], and it was recently demonstrated that *in vitro* built specific amyloid conformations sustained new phenotypic strains [15]. However, to generate these different structures, Colby et al. [15] used different conditions, decreasing urea, and/or temperature. But, we show here that structural diversity can also be generated under the same environmental conditions, a phenomenon already observed for some other amyloids [49,52]. We made a link between the heterogeneity of

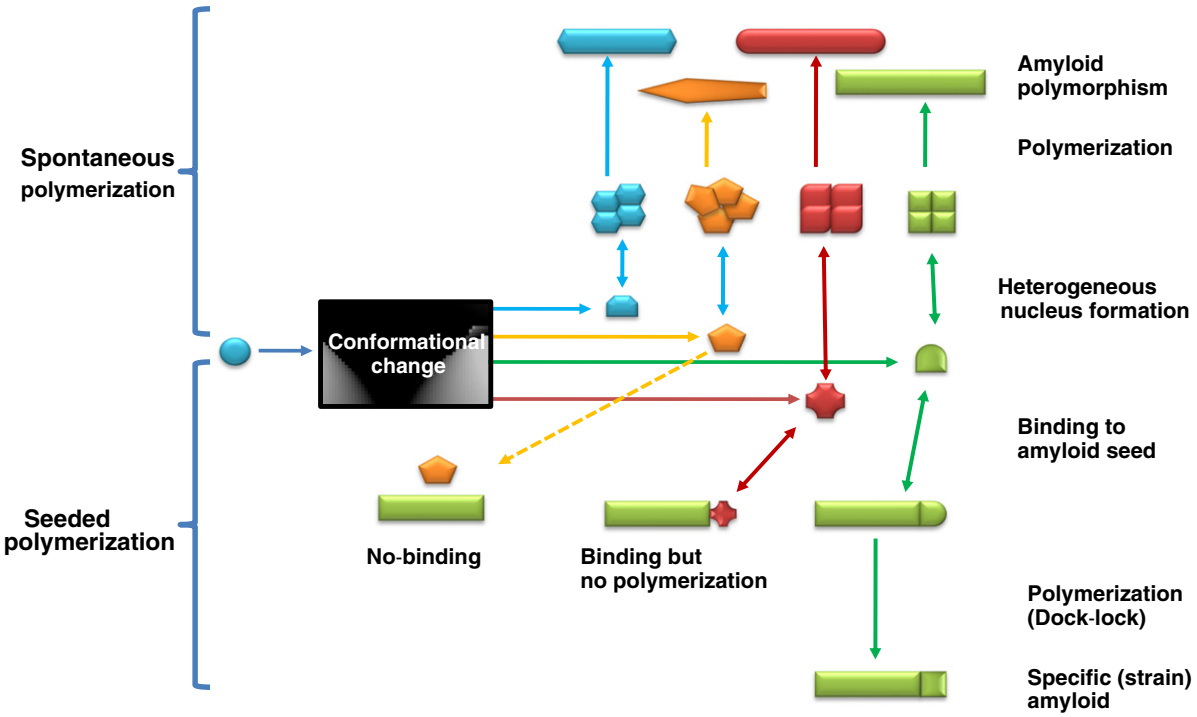

Fig. 11. Model of prion amyloid formation. Amyloidogenesis of prion protein *in vitro* is a nucleation-dependent polymerization process. However, the nucleation is not the main determinant of the lag time, another mechanism should be postulated to explain the weak dependency to the initial concentration of monomers and the residual lag time observed during seeded polymerization. This mechanism is symbolized by a black box and some hypotheses on its nature are proposed in the Discussion. The diversity of the amyloids obtained with the same purified prion protein implies the genesis of different conformers of the monomer, but only the corresponding conformer can react with a precise amyloid used for seeding. This hypothesis would explain not only the heterogeneity of amyloids but also the perpetuation of the strains and results presented here (Fig. 6C) that has shown an inverse dependency of the lag time with initial concentration at constant seed.

structures and the polymerization dynamics. We propose that the different parameters (*i.e.* the rate of polymerization and the sensitivity to agitation) are selected during nucleus formation. The important lag time heterogeneity observed (see Fig. 4) suggests that the first nucleus formed determines the characteristics of the dynamics of polymerization that are encrypted in the amyloid structure. When built, the selected structure propagates because it overcomes nucleation, and then fibril morphology is propagated to daughter fibrils by a template dependent mechanism. Such self-propagating fibril structure represents the structural basis of multiple strains of mammalian prion diseases.

It was observed during serial passage that synthetic prion went to a gradual adaptation with decreasing incubation period [14,15], and we observed a similar phenomenon by successive seeding that reduced T_{lag} and increased polymerization rate. Two interpretations can be proposed: 1/selection of the best adapted structure, *i.e.* those that multiply the most rapidly under the buffer conditions used, or 2/an adaptation of the structure, for example by extending cross-beta structure. These two explanations are not mutually exclusive. Furthermore, the decrease in the lag phase during serial passaging clearly goes against the conformational change hypothesis and argues for simple nuclear heterogeneity. However, to explain the long incubation period, Colby et al. [15] suggested that infectious amyloid is "contaminated" by a so-called intermediate (rPrP*) unfolded protein. From our results it can be proposed that a mixture of "strains" was obtained reducing the quantity of the most infectious strain.

Under the experimental conditions used in this work, there is no evident correlation between lag time and maximal rate (see Fig. 10). This observation appears in contradiction with previous reports [17,32,40,55]. Indeed, these authors have observed that the lag time is generally well correlated with the inverse of the maximal growth rate. This correlation did not appear under the experimental conditions used in our work, but putting the experimental points we have obtained into a more general graph that takes into account many independent experimental works, our results are in agreement with the previous observations [32,40] (see Supplementary data Fig. S8). What does it mean? This means that, although our results are consistent with the general phenomenon, the specificities of our experiments shed light on a phenomenon not observable when more general aspects are taken into account. According to Knowles et al. [32], when secondary nucleation pathways are active, the experimental results are primarily determined by the exponential growth regime that takes place in the initial phase of the reaction. However, the magnitude of the noise on T_{lag} for the same rate of polymerization is a very important factor. If one selects a range of rate value of 2 the T_{lag} can vary as much as 100 times, and reciprocally if one select a small interval of T_{lag}. In other words: enough variability exists in the experimental results to hide important phenomena. This is the case in our experiments. The physico-chemical conditions of polymerization remain very close in the set of experiments we present, mainly if compared with the set of results compiled by Fandrich [40] or Knowles et al. [32]. Our experimental approach appears to be more adapted to reveal marginal phenomena while compilation of heterogeneous results evidence more general phenomena. However, this marginal phenomenon allows us to shed light on an important phenomenon of the prion diseases, the production of diversity from homogeneous conditions.

Interesting consequences can be proposed in light of this work.

1. The creation of infectious prions from the recombinant protein has been rather disappointing. Although important successes have been published [14,15,56–58], most of the trials have been unsuccessful, raising the question of the reality of this phenomenon. This suggests that only some preparations are infectious. We show here that different structures can be generated from a unique starting condition. If we accept that a relation exists between

structures and strains, our results suggest that only some of the structural strains are infectious, those presenting a set of dynamics parameters in accordance with the *in vivo* polymerization. Such a set has been theoretically predicted [16] and experimentally observed for yeast prion-like elements [59] and a marked structural difference has been evidenced between infectious and non infectious prion amyloids [60]. A question remains: what are the structural characteristics that lead to infectious amyloids and how to direct *in vitro* experiment to obtain them? Are there only dynamics as proposed [59] for yeast prion, or also structural as proposed for *Podospora* prion [61,62]

2. The results presented here reveal that many different amyloid structures can be obtained with a highly purified prion protein. Changing polymerization conditions modifies the set of possible structures, and, under a single defined condition this set seems to be very large. This means that probably a huge amount of possibilities is open for new infectious amyloids emergence. As pointed out by C. Soto [63], the possibility that a new amyloid-based plague could emerge, should be taken seriously into account.

Supplementary data associated with this article can be found, in the online version, at doi:10.1016/j.bbapap.2011.05.016.

Funding

This work was supported by EC ImmunoPrion Project no. 023144 and ANR grant no. 08-JCJC-0135-01. The funders had no role in study design, data collection and analysis, decision to publish, or preparation of the manuscript.

Author contributions

Conceived and designed the experiments: J-PL. Performed the experiments: M-TA-M, PF, VZ-S, J-DA. Analyzed the data: JPL, LP-M. Developed the mathematics of the models: LP-M, EH, J-PL. Wrote the paper: J-PL and LP-M. All authors critically read and improved the manuscript.

Acknowledgments

We gratefully acknowledge the helpful assistance of Dr. A. Gross during the experiments with FACS, of Dr J. Torrent during experiments with circular dichroism and F. Godiard for help with electron microscopy. We thank Dr. Glenn Webb for his helpful comments on the manuscript.

Appendix. Derivation of the equations used to analyze the experimental results

A number of quantitative models of amyloid polymerization have been proposed (see for instance Refs. [16,17], and for a review Ref. [20]). However, the complexity of the models and the high number of independent parameters do not generally allow a complete identification of the theoretical parameters with those available by the experiments. But, the experimental methods used during this work render some simplifications available, first because of the reduced number of parameters, but also because some experimental results can be used to validate the choice of some simplifications and so reduce the complexity of more general models. The purpose of this appendix is to propose and to justify simpler models where parameters can be experimentally determined and so to analyze the *in vitro* polymerization kinetics under the experimental conditions used during this work.

Appendix A. Analysis of nucleation without polymerization

If we consider the following nucleation system

$$
\begin{aligned}
&A_1 + A_1 \underset{k_-^2}{\overset{k_+^1}{\rightleftharpoons}} A_2\\
&A_1 + A_2 \underset{k_-^3}{\overset{k_+^2}{\rightleftharpoons}} A_3\\
&\qquad\vdots\\
&A_1 + A_i \underset{k_-^{i+1}}{\overset{k_+^i}{\rightleftharpoons}} A_{i+1}\\
&\qquad\vdots\\
&A_1 + A_{n-2} \underset{k_-^{n-1}}{\overset{k_+^{n-2}}{\rightleftharpoons}} A_{n-1}\\
&A_1 + A_{n-1} \xrightarrow[k_+^{n-1}]{} A_n
\end{aligned}
$$

A_1 stands for the monomer concentration, $A_i, i=2,\ldots,n$ are the intermediate oligomers concentrations, and the k_+^i and k_-^i are the reaction rates depending on the step.

This system simulates the nucleus formation, noted A_n of size n which is the latter step, it is irreversible. At this point, we do not consider elongation after the nucleus formation.

The dynamics is described by the following differential equations

$$
\begin{cases}
\dfrac{dA_1}{dt} = -J_1 - \sum_{i=1}^{n-1} J_i\\
\dfrac{dA_i}{dt} = J_{i-1} - J_i \quad i = 2,\ldots,n-1\\
\dfrac{dA_n}{dt} = J_{n-1}
\end{cases}
\tag{A.1}
$$

with $J_i = k_+^i A_i A_1 - k_-^{i+1} A_{i+1}$ for $i=1\ldots n-2$ and $J_{n-1} = k_+^{n-1} A_{n-1}$. Equation on A.1 is deduced by the mass conservation, *i.e.*

$$
\frac{d}{dt}\sum_{i=1}^{n} iA_i = 0 \tag{A.2}
$$

Let us assume that the nucleation is well-balanced. This simplification is generally assumed by most of the models proposed [23,64]. It could be challenged *in vivo* but the homogeneity of the *in vitro* system described here justifies this hypothesis. So, we obtain the following equation regarding the quantities $i=1\ldots n-1$ at equilibrium (denoted by A_i^{eq}) we obtain from Eq. (A.1) that $J_i = J_{i-1}, \quad i = 2\ldots n-1$ and thus

$$
-J_1 - \sum_{i=1}^{n-1} J_1 = -nJ_1 = 0 \Rightarrow J_i = 0. \tag{A.3}
$$

From this system, we can compute A_{n-1}^{eq} according to A_1^{eq}, that gives

$$
A_{n-1}^{eq} = K A_1^{eq^{n-1}}. \tag{A.4}
$$

with $K = \left(\prod_{i=1}^{n-2} \dfrac{k_+^i}{k_-^{i+1}}\right)$.

If the monomer concentration is considered large enough, and the amount of monomer used for the nucleation steps is insignificant in comparison with the initial monomer concentration, then $A_1^{eq} = A_1(0) = M_0$ where M_0 is the initial concentration of monomer. This assumption is quite straightforward under the conditions used because only some nuclei are necessary to start the polymerization that is afterward sustained by secondary nucleation highly dependent of the breaking of

amyloid fibril during the vigorous stirring used during the *in vitro* polymerization. Taken into account this assumption, combined with Eq. (A.4) it gives

$$A_{n-1}^{eq} = KM_0^{n-1}. \tag{A.5}$$

Now, the time evolution of nucleus concentration is given by

$$\frac{dA_n}{dt} = k_+^{n-1} KM_0^n \tag{A.6}$$

which gives

$$A_n(t) = k_+^{n-1} KM_0^n t \tag{A.7}$$

It is then possible to deduce a lag time of nucleation (T_{nlag}) defined such that

$$nA_n\left(T_{nlag}\right) = aM_0 \tag{A.8}$$

Where a is a given fraction of the protein concentration (that can be arbitrary chosen in accordance with experimental measurement purposes) that stands for the proportion of monomers polymerized in nuclei. It needs to be small enough to be consistent with the hypothesis $A_1^{eq} \approx M_0$. Thus, T_{nlag} is given by the following expression

$$T_{nlag} = \frac{a}{nk_+^{n-1} KM_0^{n-1}} \tag{A.9}$$

and, by keeping a constant

$$log\left(T_{nlag}\right) = -(n-1)\ log(M_0) + C^{te} \tag{A.10}$$

where C^{te} is a constant.

Appendix B. Polymerization after seeding in an *in vitro* system with vigorous shaking

Let us assume that polymers of size longer than n lengthen by adding one monomer after another. Let us denote by F_i the concentration of polymers of size i, and M the monomer concentration. The lengthening is considered as an irreversible process in agreement with the Dock–Lock mechanism discussed above [65–67] and can be given by

$$F_i + M \xrightarrow{k} F_{i+1}. \tag{B.1}$$

In more general models [16,17,32] the secondary nucleation is inserted into the equations resulting from the possibility of breaking the polymer. This breaking is considered constant leading to a fibril length dependent of the monomer concentration [16,17,32] that give a good representation of *in vivo* kinetics of prion infection [68] and some *in vitro* amyloid polymerization [32]. However, under the conditions used in the experiments described in our work, under vigorous shaking, polymer breaking cannot be considered as constant, it is rapid and leads to homogeneous length of the polymer. This was experimentally proven by the measurement of the mean length of the amyloid during polymerization when concentration varies from initial concentration to zero. Indeed, the lengths remain constant throughout the experiment (see Supplemental, Fig. S9). Such a result was also obtained by Chatani et al. [69] using β2-microglobulin amyloid and ultrasonication. Thus we assume that the polymer fragmentation process occurs in such a way that it allows the fibrils to have a constant mean length N throughout the experiment. The following equation on monomers can then be deduced

$$\frac{dM}{dt} = -\sum_{1\geq n} kF_i M = -kFM, \tag{B.2}$$

with $F = \sum F_i$, is the total concentration of polymers. Let us denote by m the monomer mass (that is the number of monomers in polymers), then $m = NF$. Since the total polymer mass is conserved in the system, we have

$$\frac{dM}{dt} + \frac{dm}{dt} = 0. \tag{B.3}$$

Moreover,

$$\frac{dm}{dt} = kFM, \tag{B.4}$$

and

$$m(t) + M(t) = m_0 + M_0 \approx M_0 \tag{B.5}$$

since $m_0 \ll M_0$.

Let replace F by $\frac{m}{N}$ in Eq. (B.4) and M by $M_0 - m$. We obtain then the following differential equation on m

$$\frac{dm}{dt} = k\frac{m}{N}(M_0 - m), \tag{B.6}$$

with the initial condition at $t = T_0$, and

$$m(T_0) = m_0. \tag{B.7}$$

The solution of the logistic in Eq. (B.6) is

$$m(t) = \frac{M_0}{1 + \left(\frac{M_0}{m_0} - 1\right)e^{-\frac{k}{N}M_0(t-T_0)}}. \tag{B.8}$$

Consequently, $m(0)$ is the quantity of seeding polymers to start the experiments, and T_0 is the time when polymerization begins.

The inflection point at time T_i is:

$$Ti = T_0 + \frac{N}{kM_0}\ ln\left(\frac{M_0}{m_0} - 1\right). \tag{B.9}$$

Thus the beginning of the polymerization at time T_0 can easily be deduced from the analysis of the sigmoid. Under these conditions, if $T_0 \neq 0$, it corresponds to a residual lag time (T_{rlag}) when seeding is considered (see Fig. 1).

References

[1] S.B. Prusiner, Prions, Proc. Natl. Acad. Sci. U. S. A 95 (1998) 13363–13383.
[2] J.H. Come, P.E. Fraser, P.T. Lansbury Jr., A kinetic model for amyloid formation in the prion diseases: importance of seeding, Proc. Natl. Acad. Sci. U. S. A 90 (1993) 5959–5963.
[3] J.T. Jarrett, P.T. Lansbury Jr., Seeding "one-dimensional crystallization" of amyloid: a pathogenic mechanism in Alzheimer's disease and scrapie? Cell 73 (1993) 1055–1058.
[4] F. Ferrone, Analysis of protein aggregation kinetics, Methods Enzymol. 309 (1999) 256–274.
[5] C. Chothia, J. Janin, Principles of protein–protein recognition, Nature 256 (1975) 705–708.
[6] F. Chiti, C.M. Dobson, Protein misfolding, functional amyloid, and human disease, Annu. Rev. Biochem. 75 (2006) 333–366.
[7] B. Caughey, G.S. Baron, Prions and their partners in crime, Nature 443 (2006) 803–810.
[8] R.A. Bessen, D.A. Kocisko, G.J. Raymond, S. Nandan, P.T. Lansbury, B. Caughey, Non-genetic propagation of strain-specific properties of scrapie prion protein, Nature 375 (1995) 698–700.

[9] J. Collinge, K.C. Sidle, J. Meads, J. Ironside, A.F. Hill, Molecular analysis of prion strain variation and the aetiology of 'new variant' CJD, Nature 383 (1996) 685–690.
[10] G.C. Telling, P. Parchi, S.J. DeArmond, P. Cortelli, P. Montagna, R. Gabizon, J. Mastrianni, E. Lugaresi, P. Gambetti, S.B. Prusiner, Evidence for the conformation of the pathologic isoform of the prion protein enciphering and propagating prion diversity, Science 274 (1996) 2079–2082.
[11] D. Peretz, R.A. Williamson, G. Legname, Y. Matsunaga, J. Vergara, D.R. Burton, S.J. DeArmond, S.B. Prusiner, M.R. Scott, A change in the conformation of prions accompanies the emergence of a new prion strain, Neuron 34 (2002) 921–932.
[12] J. Collinge, A.R. Clarke, A general model of prion strains and their pathogenicity, Science 318 (2007) 930–936.
[13] J. Falsig, K.P. Nilsson, T.P. Knowles, A. Aguzzi, Chemical and biophysical insights into the propagation of prion strains, HFSP J. 2 (2008) 332–341.
[14] G. Legname, I.V. Baskakov, H.O. Nguyen, D. Riesner, F.E. Cohen, S.J. DeArmond, S.B. Prusiner, Synthetic mammalian prions, Science 305 (2004) 673–676.
[15] D.W. Colby, K. Giles, G. Legname, H. Wille, I.V. Baskakov, S.J. Dearmond, S.B. Prusiner, Design and construction of diverse mammalian prion strains, Proc. Natl. Acad. Sci. U. S. A 106 (2009) 20417–20422.
[16] M.L. Greer, L. Pujo-Menjouet, G.F. Webb, A mathematical analysis of the dynamics of prion proliferation, J. Theor. Biol. 242 (2006) 598–606.
[17] J. Masel, V.A. Jansen, M.A. Nowak, Quantifying the kinetic parameters of prion replication, Biophys. Chem. 77 (1999) 139–152.
[18] J. Masel, V.A. Jansen, Prion kinetics, Biophys. J. 87 (2004) 728 author reply 729.
[19] E.T. Powers, D.L. Powers, The kinetics of nucleated polymerizations at high concentrations: amyloid fibril formation near and above the "supercritical concentration", Biophys. J. 91 (2006) 122–132.
[20] A.M. Morris, M.A. Watzky, R.G. Finke, Protein aggregation kinetics, mechanism, and curve-fitting: a review of the literature, Biochim. Biophys. Acta 1794 (2009) 375–397.
[21] C.C. Lee, A. Nayak, A. Sethuraman, G. Belfort, G.J. McRae, A three-stage kinetic model of amyloid fibrillation, Biophys. J. 92 (2007) 3448–3458.
[22] R.F. Goldstein, L. Stryer, Cooperative polymerization reactions. Analytical approximations, numerical examples, and experimental strategy, Biophys. J. 50 (1986) 583–599.
[23] F. Oosawa, M. Kasai, A theory of linear and helical aggregations of macromolecules, J. Mol. Biol. 4 (1962) 10–21.
[24] M.T. Alvarez-Martinez, J. Torrent, R. Lange, J.M. Verdier, C. Balny, J.P. Liautard, Optimized overproduction, purification, characterization and high-pressure sensitivity of the prion protein in the native (PrP(C)-like) or amyloid (PrP(Sc)-like) conformation, Biochim Biophys Acta 1645 (2003) 228–240.
[25] I.V. Baskakov, O.V. Bocharova, In vitro conversion of mammalian prion protein into amyloid fibrils displays unusual features, Biochemistry 44 (2005) 2339–2348.
[26] J. Wall, A. Solomon, Flow cytometric characterization of amyloid fibrils, Methods Enzymol. 309 (1999) 460–466.
[27] J.W. Kelly, The alternative conformations of amyloidogenic proteins and their multi-step assembly pathways, Curr. Opin. Struct. Biol. 8 (1998) 101–106.
[28] S.R. Collins, A. Douglass, R.D. Vale, J.S. Weissman, Mechanism of prion propagation: amyloid growth occurs by monomer addition, PLoS Biol. 2 (2004) e321.
[29] S. Chen, F.A. Ferrone, R. Wetzel, Huntington's disease age-of-onset linked to polyglutamine aggregation nucleation, Proc. Natl. Acad. Sci. U. S. A 99 (2002) 11884–11889.
[30] S.B. Padrick, A.D. Miranker, Islet amyloid: phase partitioning and secondary nucleation are central to the mechanism of fibrillogenesis, Biochemistry 41 (2002) 4694–4703.
[31] E.T. Powers, D.L. Powers, Mechanisms of protein fibril formation: nucleated polymerization with competing off-pathway aggregation, Biophys. J. 94 (2008) 379–391.
[32] T.P. Knowles, C.A. Waudby, G.L. Devlin, S.I. Cohen, A. Aguzzi, M. Vendruscolo, E.M. Terentjev, M.E. Welland, C.M. Dobson, An analytical solution to the kinetics of breakable filament assembly, Science 326 (2009) 1533–1537.
[33] D.P. Hong, A.L. Fink, Independent heterologous fibrillation of insulin and its B-chain peptide, Biochemistry 44 (2005) 16701–16709.
[34] K.C. Evans, E.P. Berger, C.G. Cho, K.H. Weisgraber, P.T. Lansbury Jr., Apolipoprotein E is a kinetic but not a thermodynamic inhibitor of amyloid formation: implications for the pathogenesis and treatment of Alzheimer disease, Proc. Natl. Acad. Sci. U. S. A 92 (1995) 763–767.
[35] P. Hortschansky, V. Schroeckh, T. Christopeit, G. Zandomeneghi, M. Fandrich, The aggregation kinetics of Alzheimer's beta-amyloid peptide is controlled by stochastic nucleation, Protein Sci. 14 (2005) 1753–1759.
[36] R. Wetzel, Kinetics and thermodynamics of amyloid fibril assembly, Acc. Chem. Res. 39 (2006) 671–679.
[37] J.S. Pedersen, D. Dikov, J.L. Flink, H.A. Hjuler, G. Christiansen, D.E. Otzen, The changing face of glucagon fibrillation: structural polymorphism and conformational imprinting, J. Mol. Biol. 355 (2006) 501–523.
[38] J.S. Pedersen, D.E. Otzen, Amyloid-a state in many guises: survival of the fittest fibril fold, Protein Sci 17 (2008) 2–10.
[39] P.R. ten Wolde, D. Frenkel, Homogeneous nucleation and the Ostwald step rule, Phys. Chem. Chem. Phys. 1 (1999) 2191–2196.
[40] M. Fandrich, Absolute correlation between lag time and growth rate in the spontaneous formation of several amyloid-like aggregates and fibrils, J. Mol. Biol. 365 (2007) 1266–1270.
[41] G.W. Platt, K.E. Routledge, S.W. Homans, S.E. Radford, Fibril growth kinetics reveal a region of beta2-microglobulin important for nucleation and elongation of aggregation, J. Mol. Biol. 378 (2008) 251–263.
[42] E. Rhoades, J. Agarwal, A. Gafni, Aggregation of an amyloidogenic fragment of human islet amyloid polypeptide, Biochim Biophys Acta 1476 (2000) 230–238.
[43] P.O. Souillac, V.N. Uversky, A.L. Fink, Structural transformations of oligomeric intermediates in the fibrillation of the immunoglobulin light chain LEN, Biochemistry 42 (2003) 8094–8104.
[44] T.R. Serio, A.G. Cashikar, A.S. Kowal, G.J. Sawicki, J.J. Moslehi, L. Serpell, M.F. Arnsdorf, S.L. Lindquist, Nucleated conformational conversion and the replication of conformational information by a prion determinant, Science 289 (2000) 1317–1321.
[45] G. Bhak, J.H. Lee, J.S. Hahn, S.R. Paik, Granular assembly of alpha-synuclein leading to the accelerated amyloid fibril formation with shear stress, PLoS One 4 (2009) e4177.
[46] J.D. Green, C. Goldsbury, J. Kistler, G.J. Cooper, U. Aebi, Human amylin oligomer growth and fibril elongation define two distinct phases in amyloid formation, J. Biol. Chem. 279 (2004) 12206–12212.
[47] A. Lomakin, D.S. Chung, G.B. Benedek, D.A. Kirschner, D.B. Teplow, On the nucleation and growth of amyloid beta-protein fibrils: detection of nuclei and quantitation of rate constants, Proc. Natl. Acad. Sci. U. S. A 93 (1996) 1125–1129.
[48] R. Sabate, J. Estelrich, Evidence of the existence of micelles in the fibrillogenesis of beta-amyloid peptide, J. Phys. Chem. B 109 (2005) 11027–11032.
[49] C.S. Goldsbury, G.J. Cooper, K.N. Goldie, S.A. Muller, E.L. Saafi, W.T. Gruijters, M.P. Misur, A. Engel, U. Aebi, J. Kistler, Polymorphic fibrillar assembly of human amylin, J. Struct. Biol. 119 (1997) 17–27.
[50] A.T. Petkova, R.D. Leapman, Z. Guo, W.M. Yau, M.P. Mattson, R. Tycko, Self-propagating, molecular-level polymorphism in Alzheimer's beta-amyloid fibrils, Science 307 (2005) 262–265.
[51] W.S. Gosal, I.J. Morten, E.W. Hewitt, D.A. Smith, N.H. Thomson, S.E. Radford, Competing pathways determine fibril morphology in the self-assembly of beta2-microglobulin into amyloid, J. Mol. Biol. 351 (2005) 850–864.
[52] J. Meinhardt, C. Sachse, P. Hortschansky, N. Grigorieff, M. Fandrich, Abeta(1–40) fibril polymorphism implies diverse interaction patterns in amyloid fibrils, J. Mol. Biol. 386 (2009) 869–877.
[53] J.J. Wiltzius, M. Landau, R. Nelson, M.R. Sawaya, M.I. Apostol, L. Goldschmidt, A.B. Soriaga, D. Cascio, K. Rajashankar, D. Eisenberg, Molecular mechanisms for protein-encoded inheritance, Nat. Struct. Mol. Biol. 16 (2009) 973–978.
[54] J.L. Jimenez, G. Tennent, M. Pepys, H.R. Saibil, Structural diversity of ex vivo amyloid fibrils studied by cryo-electron microscopy, J. Mol. Biol. 311 (2001) 241–247.
[55] L. Zhu, X.J. Zhang, L.Y. Wang, J.M. Zhou, S. Perrett, Relationship between stability of folding intermediates and amyloid formation for the yeast prion Ure2p: a quantitative analysis of the effects of pH and buffer system, J. Mol. Biol. 328 (2003) 235–254.
[56] J. Castilla, P. Saa, C. Hetz, C. Soto, In vitro generation of infectious scrapie prions, Cell 121 (2005) 195–206.
[57] N.R. Deleault, B.T. Harris, J.R. Rees, S. Supattapone, Formation of native prions from minimal components in vitro, Proc. Natl. Acad. Sci. U. S. A 104 (2007) 9741–9746.
[58] F. Wang, X. Wang, C.G. Yuan, J. Ma, Generating a prion with bacterially expressed recombinant prion protein, Science 327 (2010) 1132–1135.
[59] M. Tanaka, S.R. Collins, B.H. Toyama, J.S. Weissman, The physical basis of how prion conformations determine strain phenotypes, Nature 442 (2006) 585–589.
[60] H. Wille, W. Bian, M. McDonald, A. Kendall, D.W. Colby, L. Bloch, J. Ollesch, A.L. Borovinskiy, F.E. Cohen, S.B. Prusiner, G. Stubbs, Natural and synthetic prion structure from X-ray fiber diffraction, Proc. Natl. Acad. Sci. U. S. A 106 (2009) 16990–16995.
[61] C. Ritter, M.L. Maddelein, A.B. Siemer, T. Luhrs, M. Ernst, B.H. Meier, S.J. Saupe, R. Riek, Correlation of structural elements and infectivity of the HET-s prion, Nature 435 (2005) 844–848.
[62] R. Sabate, U. Baxa, L. Benkemoun, N. Sanchez de Groot, B. Coulary-Salin, M.L. Maddelein, L. Malato, S. Ventura, A.C. Steven, S.J. Saupe, Prion and non-prion amyloids of the HET-s prion forming domain, J. Mol. Biol. 370 (2007) 768–783.
[63] C. Soto, L. Estrada, J. Castilla, Amyloids, prions and the inherent infectious nature of misfolded protein aggregates, Trends Biochem. Sci. 31 (2006) 150–155.
[64] J. Hofrichter, P.D. Ross, W.A. Eaton, Kinetics and mechanism of deoxyhemoglobin S gelation: a new approach to understanding sickle cell disease, Proc. Natl. Acad. Sci. U. S. A 71 (1974) 4864–4868.
[65] W.P. Esler, E.R. Stimson, J.M. Jennings, H.V. Vinters, J.R. Ghilardi, J.P. Lee, P.W. Mantyh, J.E. Maggio, Alzheimer's disease amyloid propagation by a template-dependent dock–lock mechanism, Biochemistry 39 (2000) 6288–6295.
[66] M. Gobbi, L. Colombo, M. Morbin, G. Mazzoleni, E. Accardo, M. Vanoni, E. Del Favero, L. Cantu, D.A. Kirschner, C. Manzoni, M. Beeg, P. Ceci, P. Ubezio, G. Forloni, F. Tagliavini, M. Salmona, Gerstmann–Straussler–Scheinker disease amyloid protein polymerizes according to the "dock-and-lock" model, J. Biol. Chem. 281 (2006) 843–849.
[67] E.P. O'Brien, Y. Okamoto, J.E. Straub, B.R. Brooks, D. Thirumalai, Thermodynamic perspective on the dock-lock growth mechanism of amyloid fibrils, J Phys Chem B 113 (2009) 14421–14430.
[68] J. Masel, N. Genoud, A. Aguzzi, Efficient inhibition of prion replication by PrP-Fc(2) suggests that the prion is a PrP(Sc) oligomer, J. Mol. Biol. 345 (2005) 1243–1251.
[69] E. Chatani, Y.H. Lee, H. Yagi, Y. Yoshimura, H. Naiki, Y. Goto, Ultrasonication-dependent production and breakdown lead to minimum-sized amyloid fibrils, Proc. Natl. Acad. Sci. U. S. A 106 (2009) 11119–11124.